ITER TASK BL 14.2: Titanium Alloys Irradiation Testing

The tensile and fatigue behavior of the titanium alloys Ti6Al4V and Ti5Al2.4Sn before and after irradiation with protons to doses up to 0.3 dpa.

Centre de Recherche en Physique des Plasmas,
Technologie de la fusion
Association Euratom- Confédération Suisse
Ecole Polytechnique fédérale de Lausanne
5232 Villigen , PSI, Switzerland

prepared by Pierre Marmy

Contributors:

Pierre Marmy
Teresa Leguey
I. Belianov
Martin Sauder*
Roland Brütsch*

* Paul Scherrer Institut, CH-5232 Villigen

Summary:

1.0 Origin, structure and chemical analysis of the alloys.

The Ti5Al2.4Sn alloy was provided by the SIBER HEGNER & CO. AG, Zürich . The origin of the material is the HOWMET Mill, USA. The material obeys the AMS 4926H specification. After hot forming, it has been annealed 1hr at 815°C and then air cooled. The finished stock is round bar of 31.75 mm. The microstructure consists of equiaxed grains of 20 μm. The chemical specification is given below.

The Ti6Al4V alloy was bought at Firth-Stahl AG, Dübendorf and comes from the TIMET, Savoie SA in UGINE, France. It was produced according to the specification WL 3.7164.1 and DIN 65040/65174 to a stock diameter of 150mm. After hot forming in the alpha + beta field, it has been annealed for 1.5 hr at 730 °C and then air cooled The structure consists of equiaxed alpha grains of about 20 μm , containing secondary alpha zones surrounded by beta phase.

Chemical compositions: [wt %]

	Al	C	Fe	Sn
Ti5Al2.4Sn	5.0	0.17	0.36	2.4
Ti6Al4V	6.08	0.0056	0.1399	-

H_2	N_2	O_2	V	Others
0.0036	0.010	0.179	-	
<0.0060	0.0065	0.176	3.95	<0.4

1.1 Microstructure of the as received alloys.

As it is typical in Ti-alloys forged in the α+β domain, the microstructure of both alloys is highly textured and will show differences depending on the orientation of observation relative to the material axis. The optical micrographs presented in Fig. 1 (Ti6Al4V) and Fig. 2 (Ti5Al2.4Sn) show the appearance of the microstructure perpendicular to the material axis.

The Ti5Al2.4Sn alloy has a globular appearance with grains mostly of the order of 20 μm. Another population of larger grains of about 40 μm or more also exist. Usually the larger grains contain smaller ones . This heterogeneity of the structure is more visible in micrographs taken along the material axis (Fig. 3,a). After etching with a solution of 10ml HF, 40ml HNO3 and 50ml H2O, lines of preferential attack appear extending along many grains(see Fig. 3, b). SEM micrographs show the different distribution of this phase for transversal and longitudinal sections, see Figs. 3c, 3d. The transversal section shows no preferred orientation, while the longitudinal section shows preferred orientation along the rod axis. EDS analysis indicates that the concentration of iron is higher than in the matrix. The total amount of this iron-rich phase was estimated to be ~1 %. Diffraction electron microscopy confirmed the b.c.c. structure of the retained phase. TEM pictures also show that the distribution is both intergranular and intragranular (Fig. 4).

The Ti6Al4V alloy has a globular structure, composed by primary grains around 20 μm and colonies of secondary elongated α grains, surrounded by intergranular β phase (Figure 2). The fraction volume of the β phase is around 13 %. Due to its different composition the β phase is quite visible at the boundaries (see Fig. 1) and appears as intergranular bands of 0.05 to 1 μm width, as it can be seen in the TEM micrographs (Fig. 5). The orientation of the secondary α grains related to the β phase obeys the Burgers relation indicating their origin as transformed products from previous β grains. There are also some small quantities of residual martensite in the larger β grains.

1.2 Experimental

1.2.2 Irradiation parameters

The specimen have been irradiated in the proton accelerator of the Paul Scherrer Institute in Villigen, Switzerland, using the PIREX irradiation facility [1]. The available beam has a maximal proton intensity of 20 μA and an energy of 590 MeV. The particularity of this type of high energy particle is to produce beside the displacement damage, also the helium typical of fusion neutrons [2].
The proton beam has a gaussian shape and is wobbled onto the specimen for getting a constant dose along the gauge length.

The mean parameters used during the titanium alloys experiments were:

Current: 14-18 μA
Beam shape: $4\sigma_{Horizontal}$=6 mm (ROUND SPECIMEN) =4mm (FLAT SPECIMEN)
$4\sigma_{Vertical}$=3mm
Wobbler amplitude: 2.5-3 mm
Wobbler frequency: 1 Hertz
Irradiation temperature: 40°C and 350°C

Mean proton flux: 1.2 10^{15} p/cm^2 sec
Mean dpa rate: 3 10^{-6} dpa/sec
Mean Helium production rate: 50 appm/dpa

1.2.3 Tensile tests:

The testing was done using a mechanical RMC100 testing machine. The tests at elevated temperature (>RT) were done into a vacuum furnace with a vacuum of the order of 10-6 mbar. Two different specimen geometries were used: the flat classical PIREX specimen with a section of 0.34x4 mm^2 and a gauge length of 5.5mm (Fig.6A) and a comparison specimen, the DIN 50125 cylindrical specimen with a diameter of 3mm and a gauge length of 18mm (Fig. 6C). The PIREX specimen is a non standard specimen designed for the irradiation with protons.
The first part of the testing was aimed at comparing these two specimen geometries in the alpha alloy, Ti 5Al2.4Sn, in order to validate the results obtained with the PIREX geometry. The tensile speed used was 0.2 to 2 %/min. The second part of the testing compares the properties of the two alloys using the PIREX specimen only at a tensile speed of 2 %/min (3x10^{-4} s^{-1})

1.2.4 Fatigue tests:

The testing was done using the same RMC100 testing machine. The tests were carried out at 350°C under vacuum, under total strain control (R=-1). The strain was measured with an automatic strain extensometer , specially designed for testing radioactive specimen. The extensometer was regularly calibrated at the test

temperature after the specimen had separated in two pieces, using a reference extensometer on the crosshead. The furnace was also regularly calibrated using thermocouples welded on the gauge length.
The specimen used for the testing is a cylindrical tubular specimen (Fig. 6B) 3.4x2.7 mm diameter with a gauge length of 5.5 mm. This specimen was specially designed for proton irradiations. The strain rate used was 0.001 to 0.002 s^{-1} (6-12%/min).
The specimen was considered as ruptured when the following condition was fulfilled (parameters given at an imposed total strain of 1%):

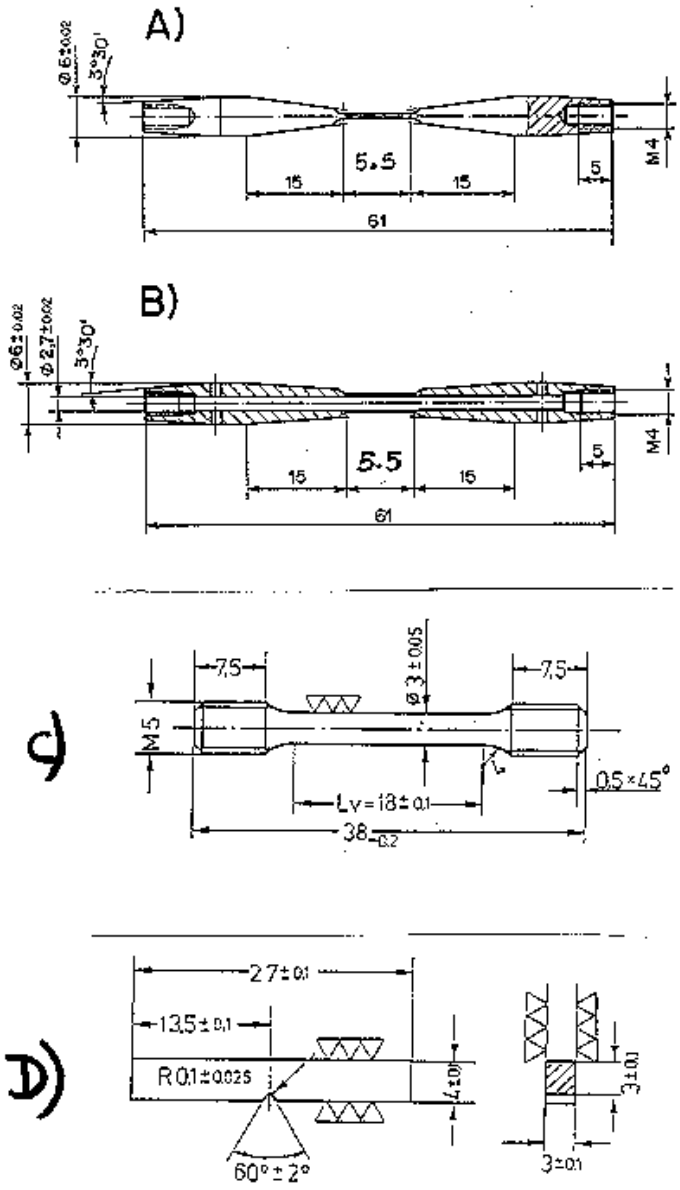

FIGURE 6: a) PIREX tensile specimen b) PIREX fatigue specimen c) DIN 50125 B3x15 tensile specimen d) DIN 50115 KLST Probe Charpy specimen

-at a stress between -35Mpa and +35Mpa , the stress/strain slope was checked and the specimen was considered ruptured if this slope was below 600Mpa/%.

The number of cycles when this condition was reached , is the number of cycles to failure Nf. Another rupture criteria was used corresponding to the number of cycles Na at which the first crack is going through the surface of the specimen. This event is detected when an inflection point appears on the compressive part of the hysteresis loop. Na was determined after the test by analysing qualitatively the registered hysteresis loops. The use of Na reduces the experimental dispersion, specially in the case of the irradiated specimen. Because of the hollow geometry of the specimen and depending of the crack orientation, crack growth up to the point when the Nf condition is satisfied, can take very long times.

1.3 Specimen Dosimetry

The dose effectively deposited onto the specimens is determined in measuring the amount of the characteristic radionuclides produced during the irradiation. The quantity of radionuclide generated during the irradiation is then used for deriving the effective fluence from the corresponding production cross section as calculated from the high energy transport code HETC. HETC delivers also a damage energy cross section for deriving the dpa's from the fluence.
The isotopes suitable for dosimetry should have a high production cross section and an half life of the order of a few years or less. Three isotopes seem interesting for Ti and Ti alloys: Na22, Ti44 and Sc46.
The results obtained for Ti44 and Sc46 are presented briefly in the Table 1 below:

Specimen Name	Integrated Fluence [A.s]	Dose Expected [dpa]	Fluence Ti44 10^{18}[p/cm^2]	Dose Ti44 [dpa]	Dose Sc46 [dpa]
I14T23	3.9	0.35	25	0.0654	0.1671
I14F21	3.4	0.31	29	0.0763	0.2257
I14F26	3.4	0.31	11	0.0298	0.1069
I25T02	3.9	0.35	64	0.1678	0.5549
I25F01	3.25	0.295	2.4	0.0063	0.0216
I25F11a	3.28	0.298	11	0.0283	0.0964
I25F11b	3.28	0.298	13	0.0341	0.1059
I14T13	2.42	0.22	18	0.0485	-
I14T01	0.136	0.01	0.94	0.0025	-
I14T02	1.058	0.10	6.2	0.0163	-

Table 1: Comparison between expected and measured doses. **14**=Ti5Al2.4Sn, **25**=Ti6Al4V

The figures from the Ti44 isotope are a factor of three below the values obtained from the Sc46. The last three specimens were irradiated before so the Sc46 radionuclide extinguished (half life=84 days). The obtained results are acceptable and the expected dose is considered as reached because:

- The specimen are cut from broken specimen with a wire saw. The cut piece is then corresponding to the end of the gauge length where the deposited dose is less.

- The production cross sections obtained from HETC and used for calculating the results are not exact values, as can be seen from the differences between Ti44 and Sc46.

1.4 Tensile tests results

1.4.1 Comparison between PIREX subsize specimen and DIN 50125 specimen

The specimen comparison was only done with the Ti 5Al 2.4 Sn alloy. Fig 7 and Fig 8 show the yield and the ultimate stress as a function of the temperature. The effect of the specimen geometry at two different strain rates (0.2 and 2 %/min) ($3x10^{-5}$ s^{-1} and $3x10^{-4}$ s^{-1}) is also reported.
In the temperature domain between RT and 300°C, the yield stress is decreasing as the temperature increases. Above 300°C and up to approximately 500 °C, a plateau is reached and the yield stress does not change much with temperature. Above 500°C , the yield stress diminishes rapidly as the temperature increases. A similar behavior is observed in Fig. 8 for the ultimate stress, although the plateau is less pronounced.
For all test temperatures, the yield and the ultimate stress increase as the strain rate is increased by a factor of 10. The effect is more apparent for the ultimate stress. The effect is also more important at room temperature.
Such a behavior of the temperature and stress sensivity indicates that the motion of dislocations is thermally activated. The appearance of a plateau indicates the presence of dynamic strain aging (DSA). In fact moderate DSA was observed at room temperature and at temperatures greater done 250°C in the flat PIREX geometry. The DIN specimen showed less DSA.
The stresses measured with the DIN specimen were higher than those measured with the PIREX geometry, at room temperature and at 400°C. In percentage the difference is about 11 and 7%, respectively. But at 200 °C, the differences were quite small.
The uniform and total elongation are shown as a function of the temperature in Fig. 9 and 5. Between RT and 400°C, uniform and total elongation are not very much sensitive to temperature. Above 400°C there is a sharp increase of the total elongation and a sharp decrease of the uniform elongation as the temperature increases.
At room temperature, the PIREX geometry gives elongation values which are too small, by almost 50% for the total elongation and 30% for the uniform elongation. From 200°C and above, the comparison is better although generally the values indicated by the DIN specimen are always higher.
The general behavior of the mechanical parameters shown in Fig. 7,8,9,10 seems to indicate that around 200°C an important physical mechanism takes place, such as the diffusion of a particular atom specie or another phenomena influencing dislocation glide.

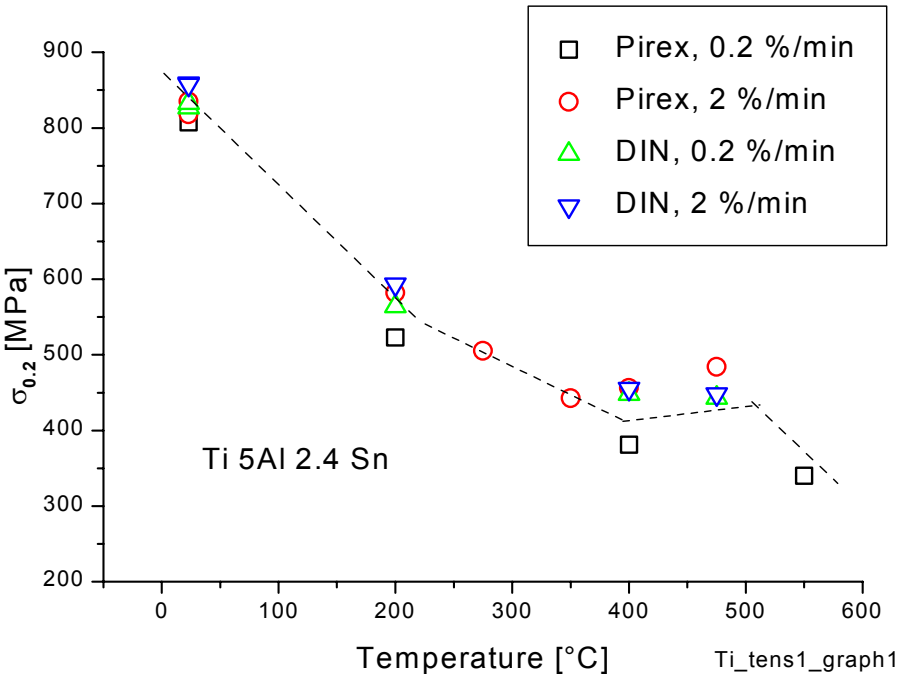

FIGURE 7: The yield stress as a function of temperature for the DIN 50125-B3x15 and the PIREX specimen at two different tensile speeds.

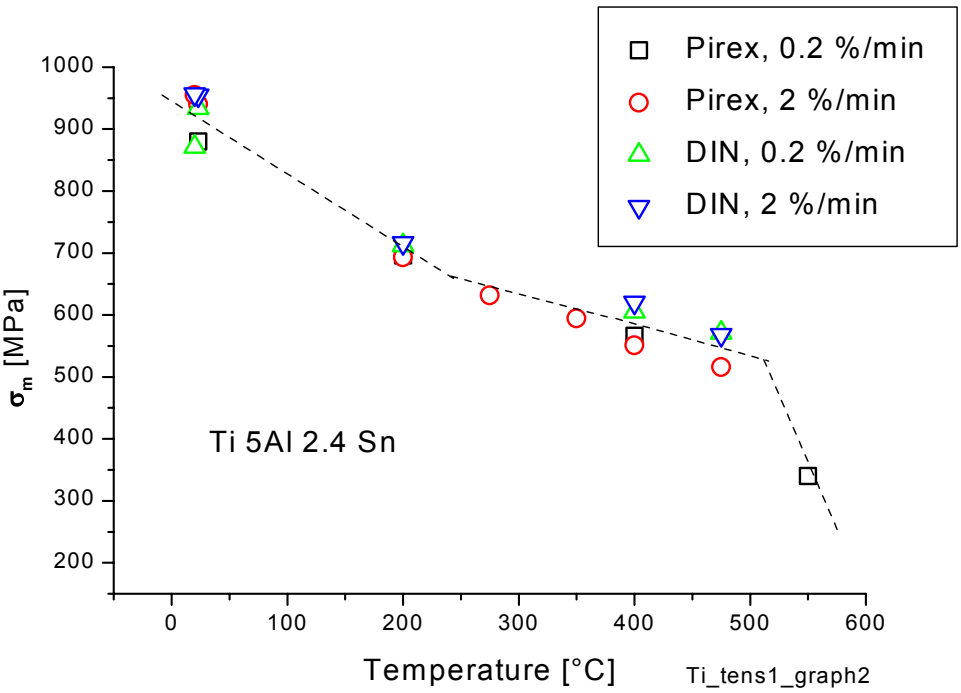

FIGURE 8: The ultimate stress as a function of temperature for the DIN 50125-B3x15 and the PIREX specimen at two different tensile speeds.

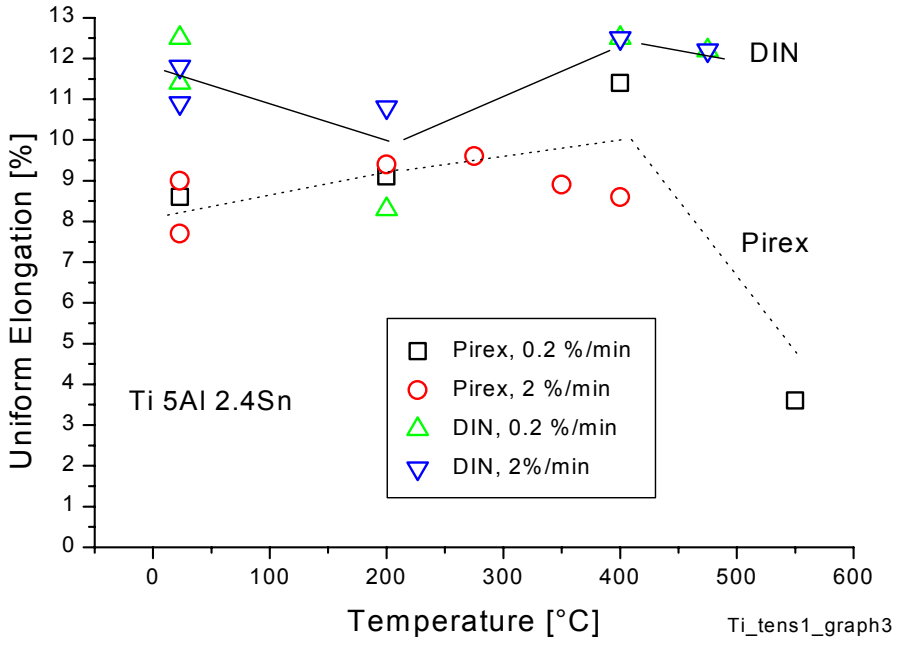

FIGURE 9: The uniform elongation as a function of temperature for the DIN 50125-B3x15 and the PIREX specimen at two different tensile speeds.

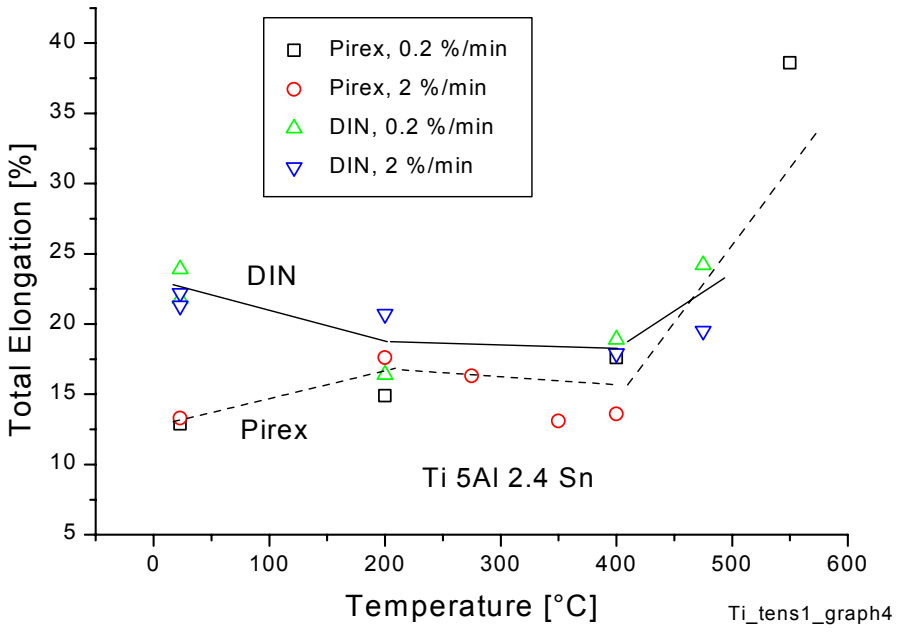

FIGURE 10: The total elongation as a function of temperature for the DIN 50125-B3x15 and the PIREX specimen at two different tensile speeds.

1.4.2 The tensile behavior of Ti5Al2.4Sn and Ti6Al4V alloys

The behavior of the yield stress and ultimate stress as a function of the temperature is reported in Fig.11 and 12 for both alloys, tested at 2%/min. Both alloys show tensile strengths higher or similar to those observed in low activation ferritic martensitic steels. Fig.13 compiles all tensile parameters of both Ti alloys and also shows the typical yield stress behaviour of 9Cr-1Mo FM steels, as a comparison.

At low temperatures (up to 150°C) the alpha alloy Ti5Al2.4Sn is slightly superior to the alpha+beta alloy Ti6Al4V whereas at higher temperatures (from 300°C) the alpha+beta alloy seems to overtake the alpha alloy.

The tensile test have demonstrated good ductilities for both alloys.Fig. 13 shows the comparison of the ductilities measured in both alloys, as a function of the test temperature. The uniform elongation A_g is slightly lower in the alpha+beta alloy as compared to the alpha alloy. Correspondingly, the situation is reversed in terms of total elongation A.

The resistance of the alloys to an anneal of 5hrs at 750°C (heat treatment necessary to load hydrogen) has been tested for both alloys. The result is also shown in Fig, 11 and 12. The Ti6Al4V alloy does not show any change. The alpha alloy Ti5Al2.4Sn is responding to the treatment in showing a reduced strength and improved ductility. The deformation curve is shown in Fig.14.

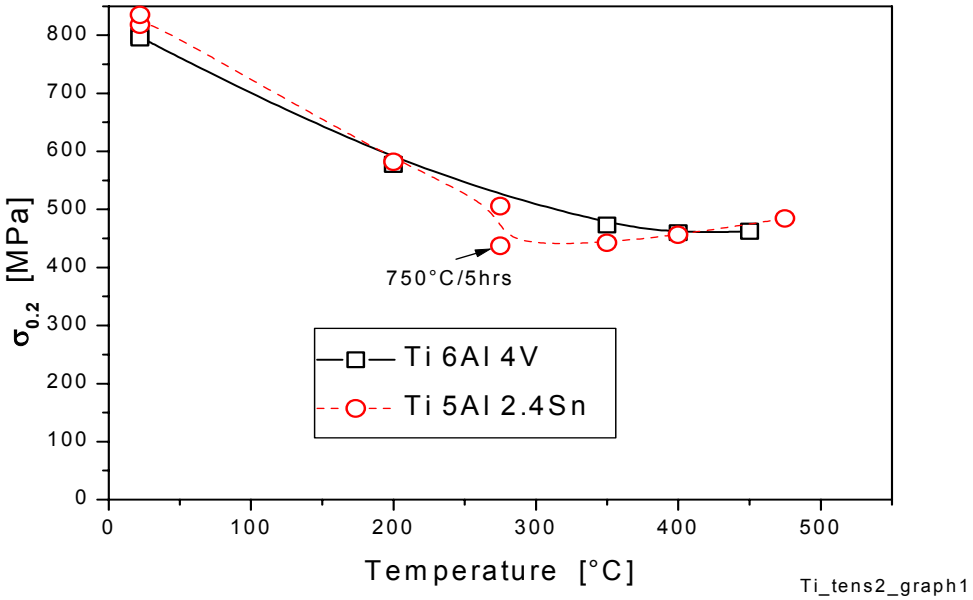

FIGURE 11: The yield stress $\sigma_{0.2}$ as a function of the temperature at a strain rate of 2%/min

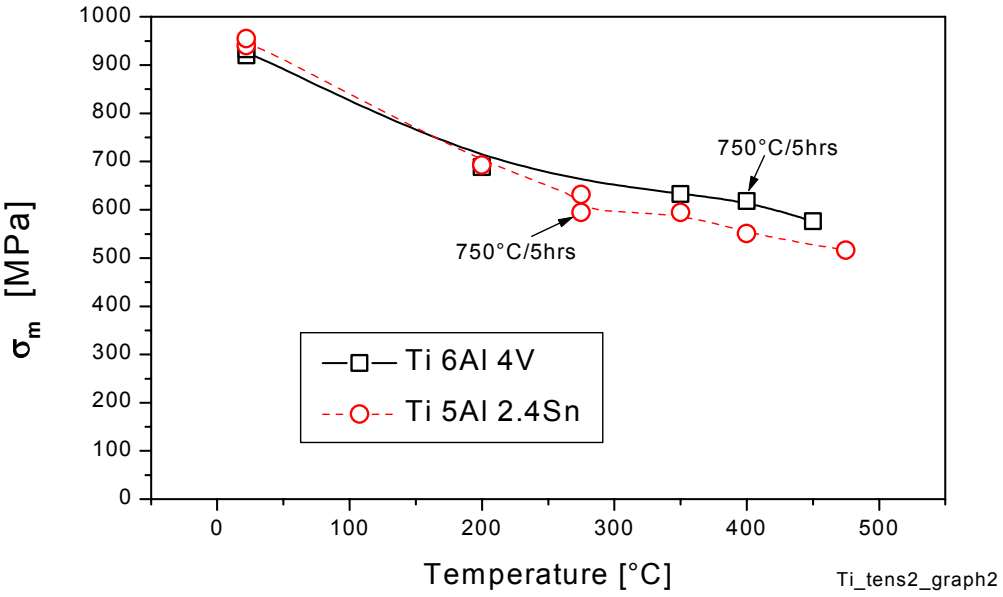

FIGURE 12: The ultimate stress σ_m as a function of the temperature at a strain rate of 2%/min

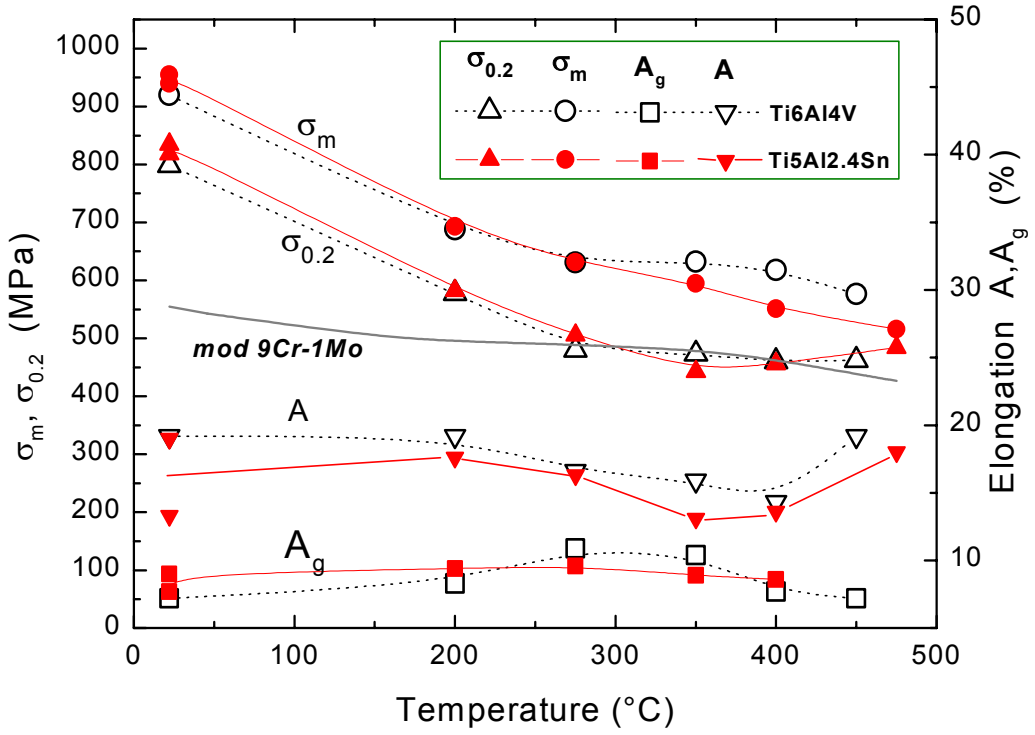

FIGURE 13: The tensile parameters of both Ti-alloys as a function of the temperature at a strain rate of 2%/min. The yield stress of typical low activation FM steels is shown for comparison.

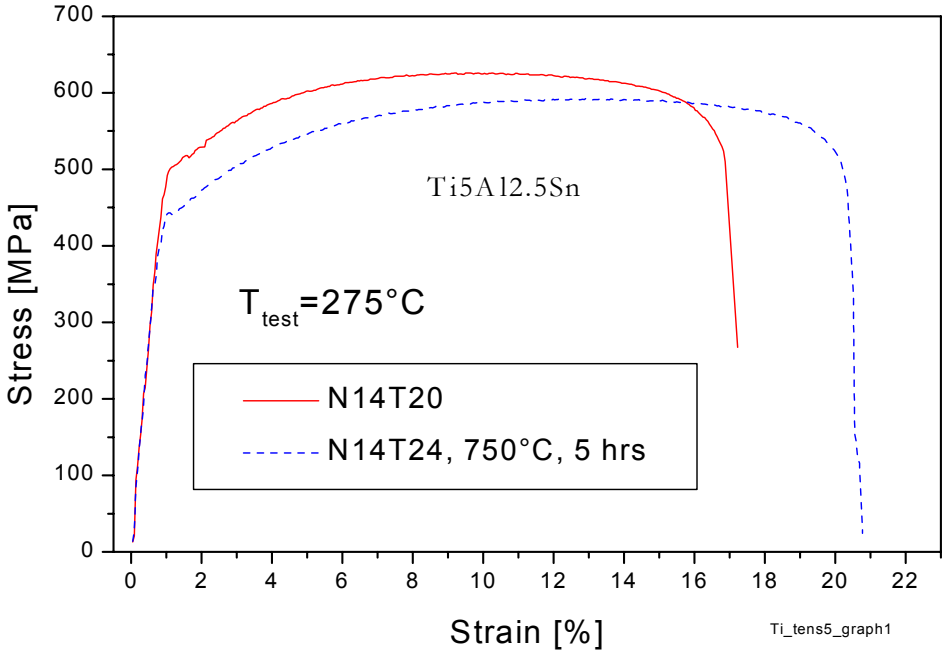

FIGURE 14. Tensile deformation curve after 5hrs/750°C. Test temperature:275°C. Ti5Al2.4Sn

1.4.3 Microstructure after tensile deformation.

The tensile specimens of Ti5Al2.5Sn alloy show a very high density of a-type straight screw dislocations **b**=1/3 <1 1 $\bar{2}$ 0> , together with parallel arrays of shorter c-component dislocations with Burgers vector **b**=1/3 <1 1 $\bar{2}$ 3> The same is observed in the primary alpha grains of the Ti6Al4V alloy.
Subgrains and deformation bands are also observed.
Fig.15 shows a few TEM micrographs from a Ti5Al2.5Sn specimen tensile tested at room temperature. Fig 16 shows some features of the microstructure after tensile deformation of a Ti6Al4V specimen at 350 °C.

1.4.4 The effect of the irradiation on strength and ductility.

1.4.4.1 Irradiation hardening and ductility

The unirradiated and irradiated tensile properties of both alloys are reported in the Table 2, on next page. For both alloys the main effect of the irradiation is to increase the stress level and reduce the ductility. But the effects are much stronger in the alpha+beta alloy as can be seen in Fig. 17 , which shows the deformation curves obtained at room temperature after irradiation at 350°C to 0.3dpa. The irradiation hardening of the alpha beta alloy remains very high at a test temperature of 350°C (see Fig. 18).
The amount of irradiation hardening observed in the Ti5Al2.4Sn irradiated at 350°C is small . The strength is also not very much affected by an irradiation at 40°C as can be seen in Fig. 19. But the ductility is reduced about 15% after 0.01dpa (Fig.19).
The behavior of the yield and ultimate stress before and after irradiation is indicated in Figs 20, 21 and 22, as a function of the test temperature.
The high temperature irradiation (Figs 20 and 21) influences both the yield and ultimate stress and the measured irradiation hardening is independent on temperature. This behavior is athermal in nature and the dislocation glide is affected by long range obstacles.
The low temperature irradiation (Fig. 22, Ti5Al2.4Sn) affects mainly the yield stress and no temperature dependence is found, indicating again an athermal hardening. The ultimate stress increases only by a few Mpa's. This can be related to an apparent strong reduction of the strain hardening capability, probably due to a reduced dislocation mobility. It is consistent with the observed reduction of ductility after irradiation (Fig. 19).

TABLE 2: Tensile properties of titanium alloys

14=Ti5Al2.4Sn 25=Ti6Al4V

(Units:Mpa,%,°C,%/min)

Specimen used: DIN 50125 B3x15, gauge length=18mm, diameter 3mm

Spec. Name	Temperature	$\sigma_{0.2}$	σ_m	Ag	A	Streck Grenze	Air Vacuum	Tensile Speed	DSA
N14D1	23	827	934	12.5	23.9	yes	air	0.2	no
N14D2	24	859	954	11.8	22.2	yes	air	1.85	no
N14D9	20	857	956	10.9	21.3		vacuum	1.51	
N14D10	21	833	871	11.4	21.8		vacuum	0.2	
N14D3	200	564	712	8.3	16.4	yes small	vacuum	0.2	no
N14D4	200	593	716	10.8	20.7	yes	vacuum	1.9	no
N14D5	400	455	620	12.5	17.9	no	vacuum	1.9	very W
N14D6	400	448	605	12.5	18.9	no	vacuum	0.2	W
N14D7	475	448	568	12.2	19.5	no	vacuum	1.9	W
N14D8	476	443	571	12.2	24.2	no	vacuum	0.2	v. very W

Specimen used: PIREX 2-177 837, gauge length=5.5mm, section 4x0.33mm

Spec. Name	Temperature	$\sigma_{0.2}$	σ_m	Ag	A	Streck Grenze	Air Vacuum	Tensile Speed	DSA
N14T10	23	807	880	8.6	12.9	yes	air	0.25	v. very W
N14T8	23	818	940	7.7	13.3	yes	air	1.61	v. very W
N14T5	200	582	693	9.4	17.6	yes	vacuum	1.72	v. very W
N14T6	200	523	696	9.1	14.9	yes	vacuum	0.22	v. very W
N14T9	400	381	566	11.4	17.6	yes	vacuum	0.21	no
N14T14	400	456	551	8.6	13.6	yes	vacuum	2	no
N14T18	22	834.8	954.7	9	19	no	air	1.733	W
N14T20	275	505.4	631.5	9.6	16.3	no	vacuum	1.88	v. very W
N14T19	350	442.4	594.6	8.9	13.1	no	vacuum	1.7	v. very W
N14T11	475	484	516		18	yes	vacuum	2	no
N14T16	550	340	327	3.6	38.6	yes	vacuum	0.18	M
N14T24	275	437	595.3	12.15	19.65	yes	vacuum	1.61	v. very W
I14T23	21.5	891.3	989.9	8	15.8	no	air	1.97	W
I14T22	200	625.9	743.7	6.5	11.2	no	vacuum	2.3	W-M
I14T21	350	481.3	628.8	6.6	9.7	no	vacuum	1.6	very W
I14T01	21	837.1	918.5	6	15.6	no	air	1.85	very W
I14T02	21	890.8	955.4	4.8	15.2	no	air	1.96	W
I14T04	200	635.1	695.6	5.1	12.1	no	vacuum	1.86	W
I14T03	350	469.05	609.5	7	11.3	no	vacuum	0.94	W
I14T13	200	567	619.3	5.4	12.35	no	vacuum	1.84	v. very W

Specimen used: PIREX 2-177 837, gauge length=5.5mm, section 4x0.33mm

Spec. Name	Temperature	$\sigma_{0.2}$	σ_m	Ag	A	Streck Grenze	Air Vacuum	Tensile Speed	DSA
N25T4	22	795	932.6	4.1	15.5	no	air	1.23	v. weak
N25T7	22	798.6	919.8	7.23	19.2	no	air	2	v. weak
N25T5	200	577.3	688.1	8.3	19.2	yes	vacuum	2.23	v. weak
N25T11	275	480	630.8	10.9	16.6	no	vacuum	1.81	weak
N25T6	350	472.8	632.2	10.36	15.9	no	vacuum	1.94	no
N25T8	450	462	576.4	7.23	19.2	no	vacuum	1.99	no
N25T9	400	459.8	618	7.72	14.3	no	vacuum	1.6	no
I25T2	21.5	1168	1216	2.9	5.72	no	air	1.7	no
I25T3	200	895.7	959.3	3.64	6.64	no	vacuum	1.8	v. weak
I25T1	350	755.4	841.7	3.3	5.06	no	vacuum	1.7	no

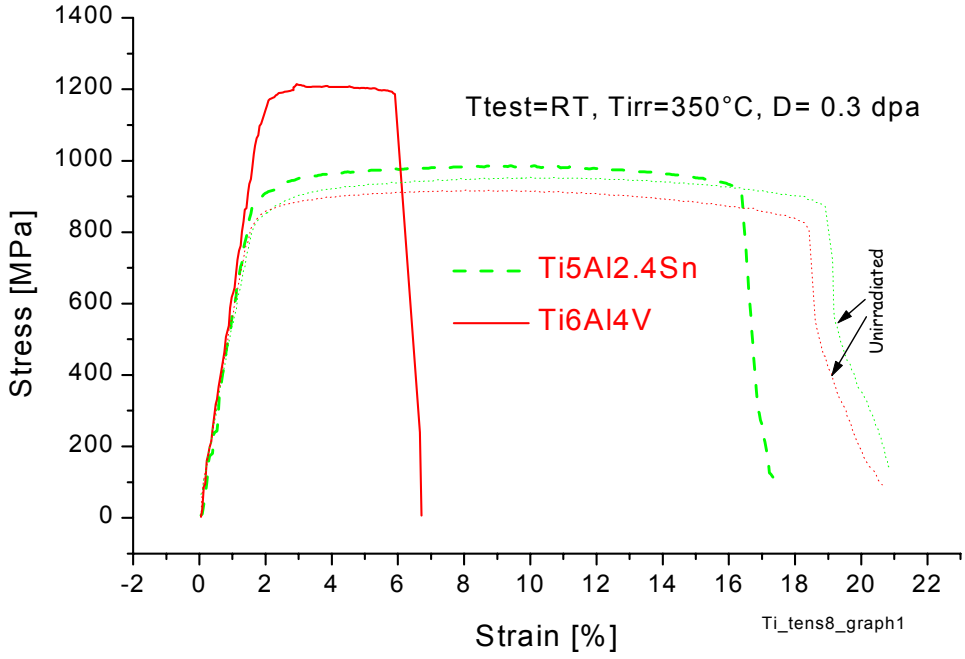

FIG. 17: Deformation curves before and after irradiation obtained at room temperature

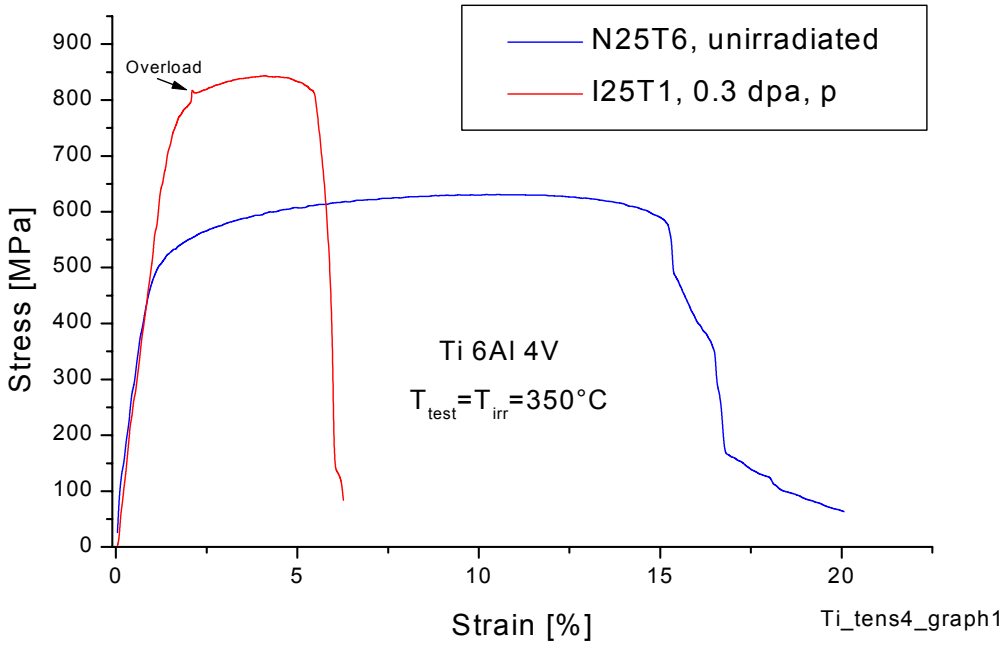

FIG. 18: Deformation curves of irradiated and unirradiated Ti6Al4V tested at 350°C

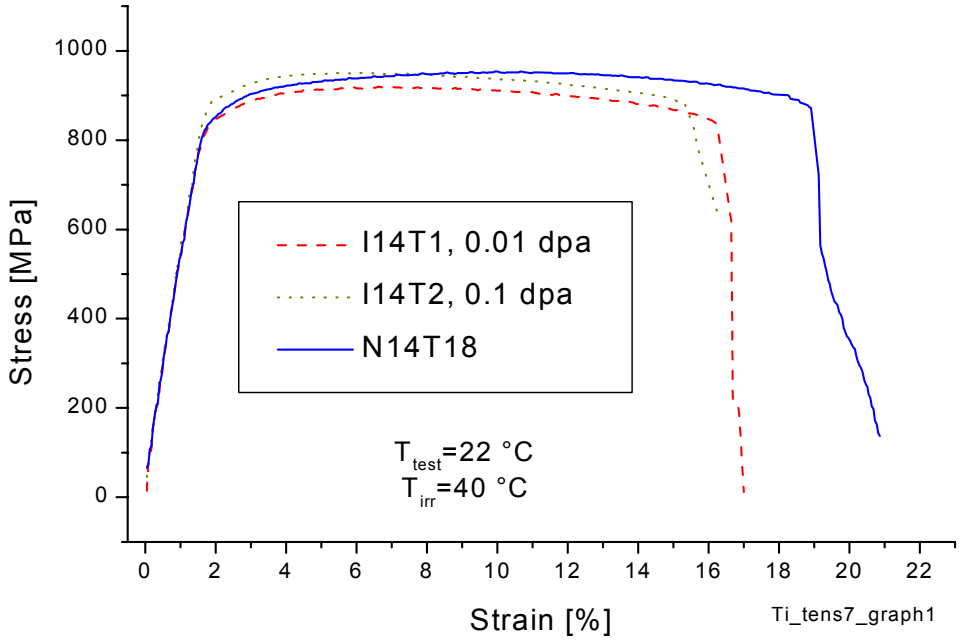

FIG. 19 Deformation curves of Ti5Al2.5Sn after irradiation at 40°C

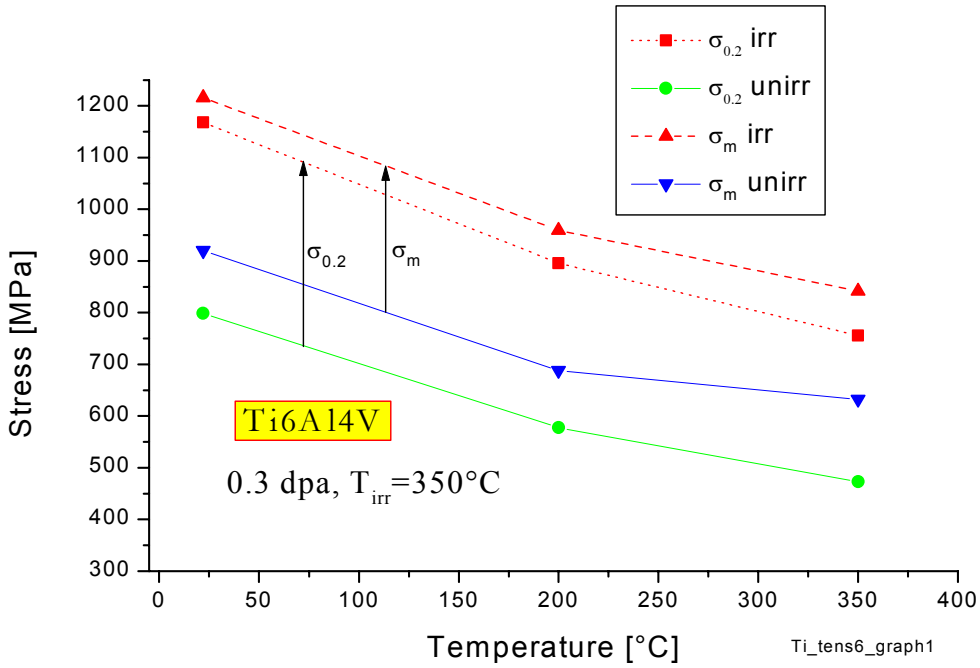

FIG. 20 The effect of the irradiation on the yield and ultimate stress in Ti6Al4V irradiated at 350°C.

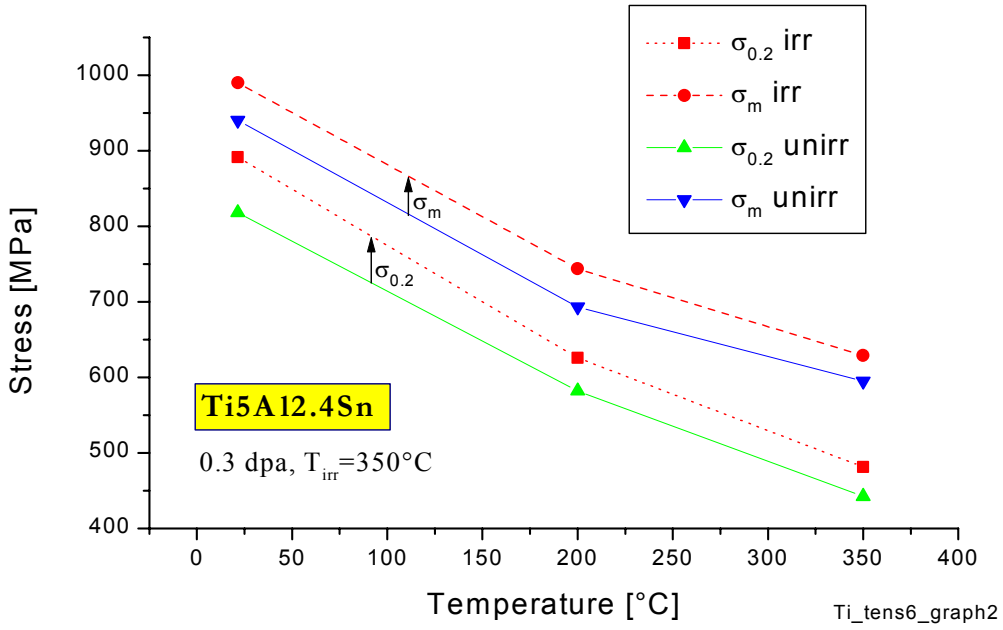

FIG. 21 The effect of the irradiation on the yield and ultimate stress in Ti5Al2.4Sn irradiated at 350°C.

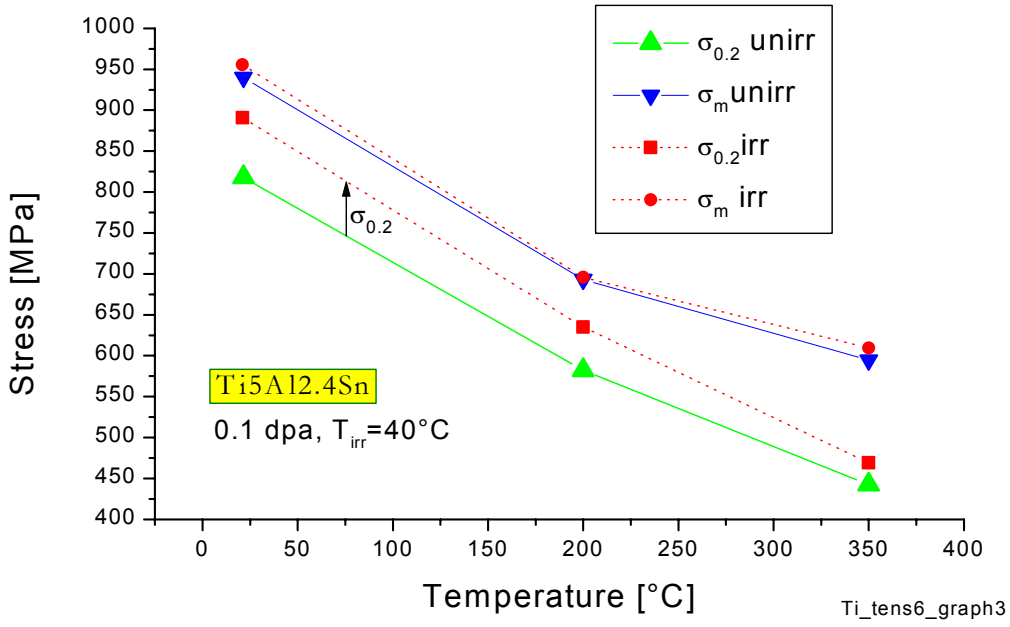

FIG. 22 The effect of the irradiation on the yield and ultimate stress in Ti5Al2.5Sn irradiated at 40°C.

1.4.4.2 Effect on strain flow

The appearance of a yield point (Streckgrenze) on the deformation curve has been reported in Table 2, for all tested specimen. Ti5Al2.5Sn presents a yield point when tested with the PIREX flat geometry (5.5x4x.33mm, Fig 6a). This yield point disappears completely when tested after irradiation in the same geometry.
The phenomenon of the yield stress is connected with the formation of solutes atmospheres around the dislocation. The anchored dislocations only move when the stress has reached a sufficient level. The irradiation could have the effect to lower the concentration of solid solution solutes by attracting them to the defect clusters. Another explanation could be that the yield point simply disappears because the irradiation induced strength increase hides the yield point.

Another interesting point is the influence of irradiation on the dynamic strain aging (DSA) behavior of the alpha alloy Ti5Al2.5Sn. In Table 2 the DSA intensity has been reported qualitatively for all test conditions with a scale going from v.very W (only little irregular perturbations of the strain flow) to S (strong and regular fluctuations of the strain-stress flow). In the unirradiated specimens, DSA of intensity M (medium) was observed only at 550°C. It seems that the domain of established DSA starts only at relatively high temperatures in titanium. Table 2 shows that the irradiation is enhancing the strain flow instabilities at relatively low temperatures between RT and 350°C. This effect is probably connected to the fact that the irradiation is promoting localized flow and therefore helps the appearance of deformation instabilities.

1.5 Fatigue tests results

1.5.1 General behavior

The fatigue testing presented in this work was done under total strain range control. Since titanium alloys are very elastic (E=120000 MPa) and very strong, the elastic contribution of the total strain is much larger than the plastic contribution. Because low cycle fatigue (LCF) requires plastic deformation, the testing of titanium alloys demands very high total strain ranges. The lower limit of the total strain range measured corresponds to fatigue lives around 10000 cycles and the upper bound was limited by the stability of the fatigue specimen used (Fig. 6b). For the alloys studied, the practicable range of the total imposed strain was found to be between 1 and 2%.

In order to check the system, the first tests were done at room temperature using the alpha alloy. It was found that this particular temperature is not suitable for LCF because due to the very high flow stresses, a nascent crack would immediately propagate through the thin cross section of the tubular specimen and induce a sudden failure.
From 200°C, a normal crack growth behavior is found and LCF tests can be carried out. All the testing was then done at the second temperature requested by the ITER Task BL14.2, which is 350°C.
The LCF test matrix is shown in Table 3.

Table 3: Results of Fatigue Tests

Units are %, s-1, Mpa, °C

Na:Number of cycle to crack initiation **Nf**: Number of cycle to fracture
14=Ti5Al2.5Sn **25**=Ti6Al4V
Strain rate= 0.001-0.002

Specimen name	Test temperature	Atmosphere	Total Imposed Strain	Na	Nf	Stress Amplitude at first cycle	Stress Amplitude at half life	Plastic Strain at half life	Type of failure
N14F20	21	air	1.4	1673	1673	1609			brittle
N14F19	21	air	1.4	284	284	1551			brittle
N14F6 β	21	air	1.4	397	1159	1538			ductile
N14F7 β	21	air	2	107	107	1724			brittle
N14F27	350	vacuum	1	10254	13476	919	846.6	0.089	ductile
N14F25	350	vacuum	1.15	3273	3656	958.6	874.3	0.251	ductile
N14F23	350	vacuum	1.3	2468	2852	962.1	891.4	0.375	ductile
N14F22	350	vacuum	1.4	1555	2078	985.3	877.3	0.453	ductile
N14F24	350	vacuum	1.5	1224	1456	992	889.3	0.573	ductile
N14F28	350	vacuum	1.8	880	986	1026	914	0.774	ductile
N14F34	350	vacuum	2	708	761	1048	946.4	0.987	ductile
N14F33	200	vacuum	1.6	1848	2030	1261	1012	0.581	ductile
I14F1	200	vacuum	1.1	2965	7949	1105	998.3	0.132	ductile
I14F2	200	vacuum	1.6	1456	1969	1428	1104	0.552	ductile
I14F21	350	vacuum	1	7200	12490	908.6	882.4	0.0895	ductile
I14F32	350	vacuum	1.1	2178	3721	1031	914.5	0.124	ductile
I14F37	350	vacuum	1.2	3920	6064	1094	944.9	0.218	ductile
I14F29	350	vacuum	1.2	2970	5619	1028	904.7	0.216	ductile
I14F30	350	vacuum	1.3	2205	2853	1080	928.6	0.314	ductile
I14F39	350	vacuum	1.5	846	1177	1108	958.4	0.494	ductile
I14F26	350	vacuum	1.8	643	667	1178	991.6	0.707	ductile

Specimen name	Test temperature	Atmosphere	Total Imposed Strain	Na	Nf	Stress Amplitude at first cycle	Stress Amplitude at half life	Plastic Strain at half life	Type of failure
25F13	350	vacuum	1.4	1118	1490	1110	1090	0.401	ductile
25F14	350	vacuum	1.2	2850	3044	1071	1041	0.198	ductile
25F15	350	vacuum	1	8348	9676	1000	994	0.0656	ductile
25F18	350	vacuum	1.8	435	501	1134	1106	0.712	ductile
25F6	350	vacuum	1.1	8765	10812	1027	1039	0.0966	ductile
25F17	350	vacuum	1.3	3550	4507	1040	1054	0.256	ductile
25F19	350	vacuum	1.6	397	784	1083	1012	0.519	ductile
25F20	350	vacuum	2	352	445	1110	1081	0.876	ductile
I25F9	350	vacuum	1	8125	8523	1064	1063	0.0322	ductile/bri
I25F11	350	vacuum	1.1	6640	7134	1141	1111	0.03	ductile
I25F7	350	vacuum	1.2	940	3208	1275	N/A	N/A	ductile
I25F01	350	vacuum	1.3	448	448	1385	N/A	N/A	brittle
I25F02	350	vacuum	1.4	815	925	1431	1328	0.185	ductile
I25F8	350	vacuum	1.6	155	155	1459	N/A	N/A	brittle
I25F3	415	vacuum	1.14	800	1468	1102	1123	0.03	ductile

1.5.2 Cyclic softening behavior

1.5.2.1 Unirradiated material

Fig. 23 shows the behavior of the total stress range and the plastic strain range as a function of the number of cycles to failure for both alloys, tested at a high imposed strain. In the case of the Ti6Al4V alloy stress and strain are almost constant over the number of cycles. But for the Ti5Al2.4V , the stress diminishes and the plastic strain increases as a function of the cycles, thus indicating that some softening is taking place.
Fig. 24 shows the behavior of both alloys when they are tested at a low imposed strain. Up to about 800 cycles , both alloys show cyclic softening. The softening is higher in the alpha alloy. Above 800 cycles, cyclic hardening is observed. The cyclic hardening is higher in the alpha+beta alloy than it is in the alpha alloy. In the Ti 6Al 4V the stress at the end of life reaches the level it had at the first cycle.
The total stress range is shown in Fig. 25 as a function of the imposed strain, at first cycle and at half life for both alloys. The difference between both curves represents the softening at half life. In the alpha alloy the softening increases slightly as the imposed strain increases. The softening is relatively important and is of the order of 80-100 MPa. In the alpha +beta alloy the softening at half life is absent at low imposed strains but a value of 75 MPa is measured at 1.6%.
The softening is more important in the alpha alloy as compared with the alpha+beta alloy Fig.25 shows also that the cyclic stresses are about 15% higher in the alpha+beta alloy.

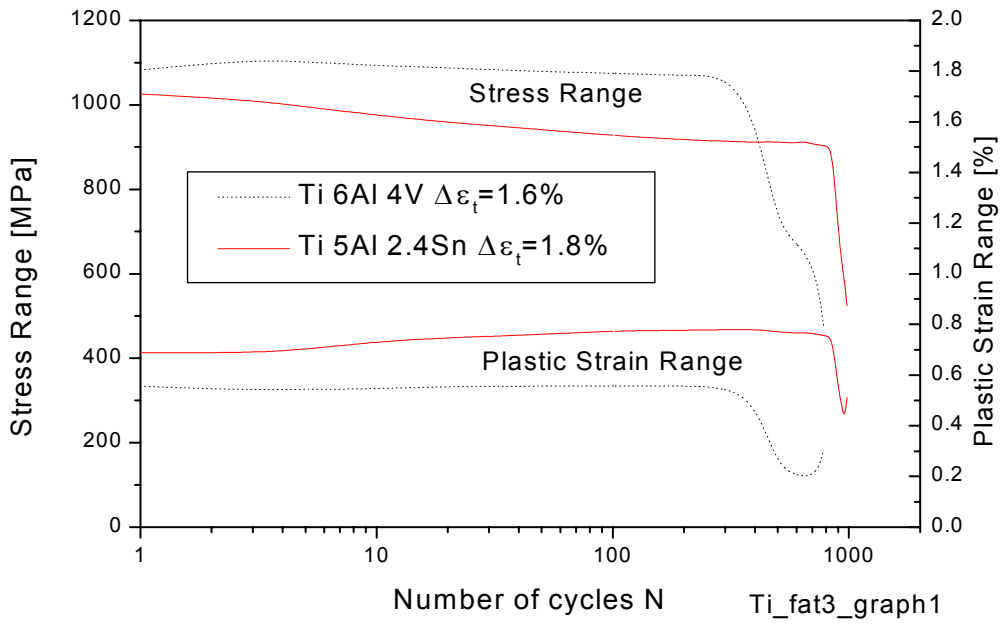

FIGURE 23: Softening behavior at a high imposed strain. T = 350°C

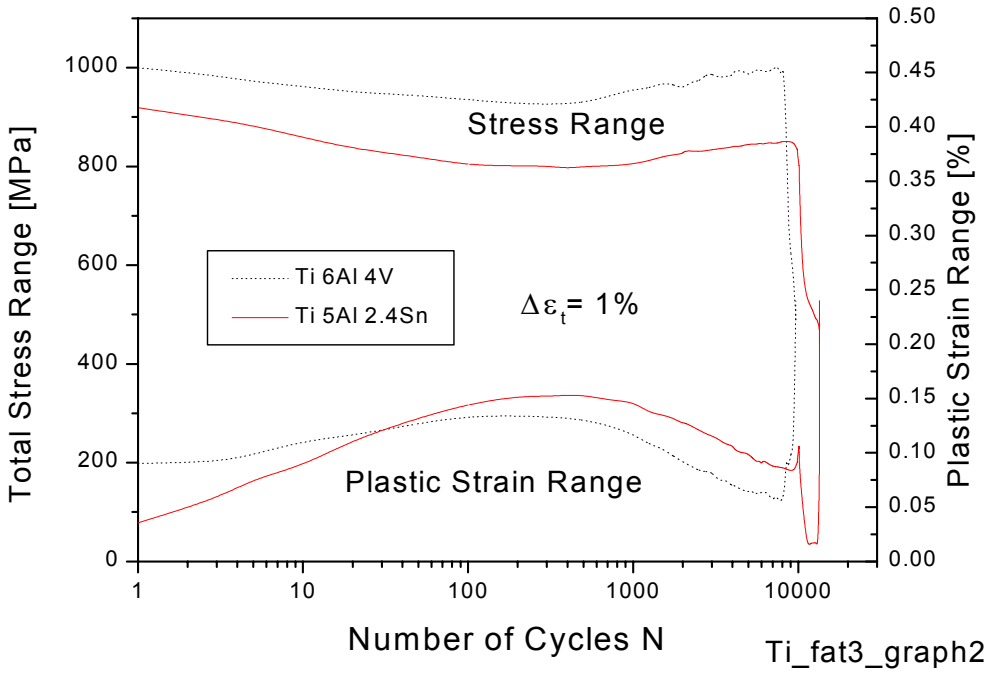

FIGURE 24: Softening behavior at a low imposed strain. T = 350°C

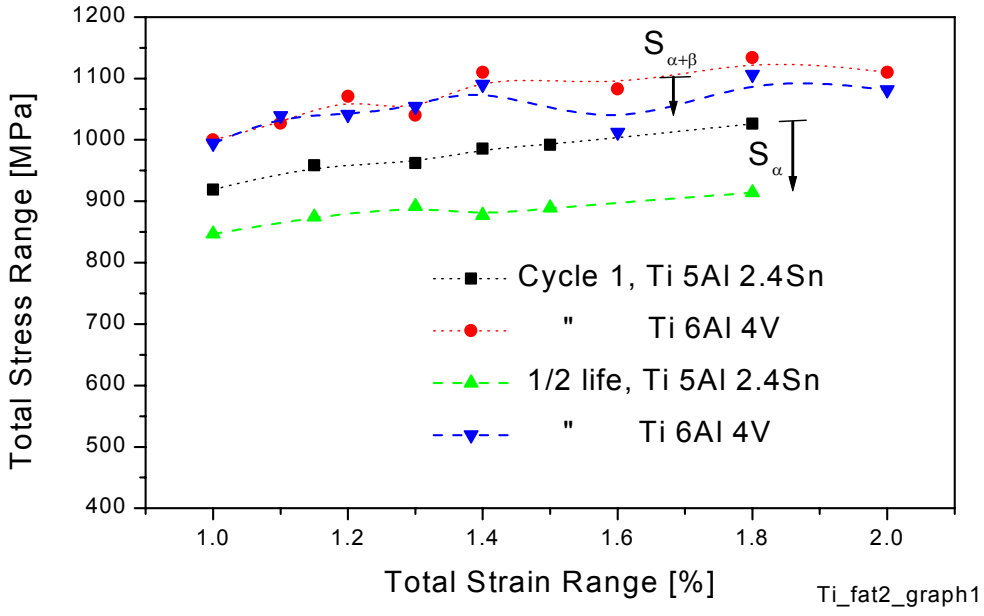

FIGURE 25: The total stress range as a function of the imposed strain range

1.5.2.2. Irradiated material

The cyclic softening behavior of the irradiated material (p,0.3 dpa,T_{irr}=350°C) is shown in Figs 26 and 27, for respectively a low and a high imposed strain. In the irradiated material a monotonic cyclic softening is observed for the case of a high imposed strain , in both materials. It is important to point out the very different behavior of the plastic strain range, in both alloys. The continuously increasing plastic strain range measured in the alpha+beta alloy is much higher as compared with the plastic range observed in the alpha alloy. The increased plasticity is probably due to the higher stress level of the cyclic stress. The higher stress is caused by the higher irradiation hardening sensitivity of the alpha+beta alloy, as shown in the preceding section.

In the case of a low imposed total strain (1%), the cyclic softening is absent in the Ti6Al4V alloy. This is because the stress is fully elastic as can be seen from the very small measured plastic strain range (Fig.26). The Ti5Al2.5Sn shows a monotonic softening with increasing plasticity.
Figs 28 and 29, show the comparison between the irradiated and unirradiated Ti-alloys. The figures indicate clearly that the secondary hardening disappears in both materials after the proton irradiation.

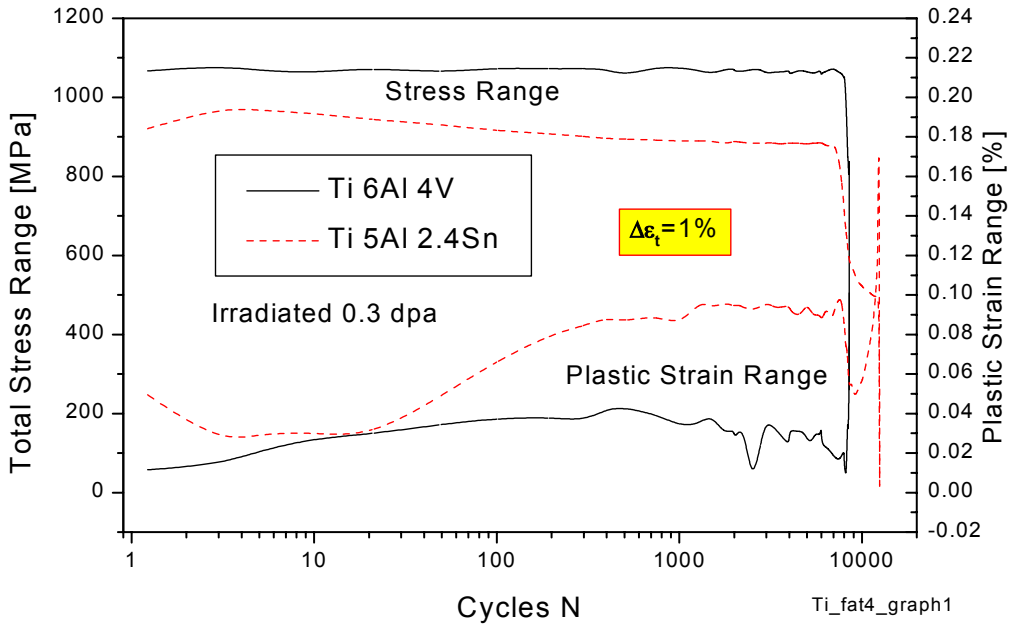

FIGURE 26: The total stress range and the total plastic range as a function of the number of cycles. Irradiated material, 0.3dpa, T_{irr}=350°C

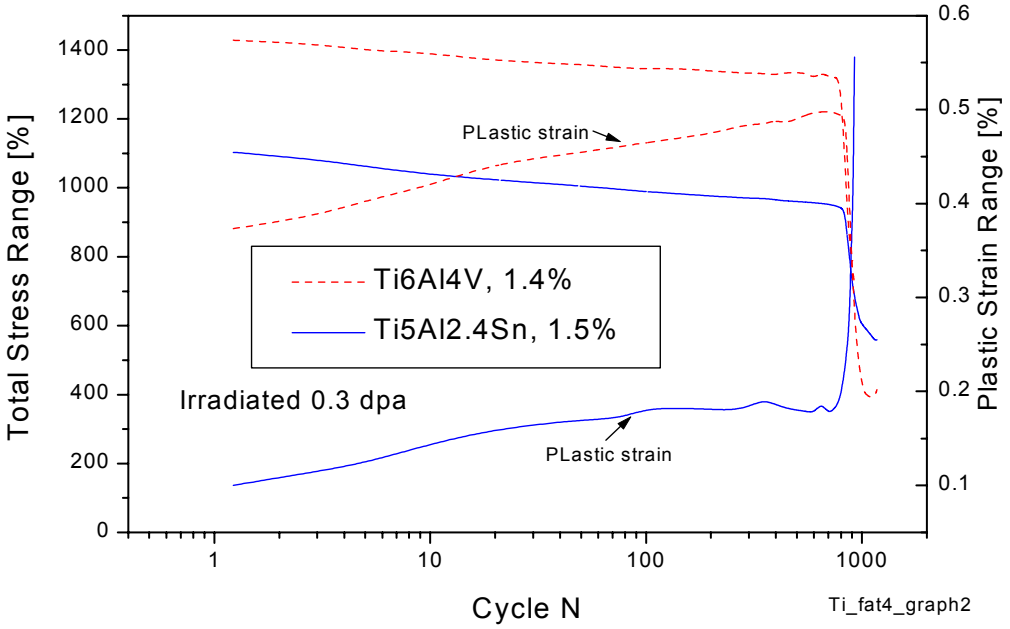

FIGURE 27: The total stresss range and the total plastic range as a function of the number of cycles. Irradiated material, 0.3dpa, T_{irr}=350°C

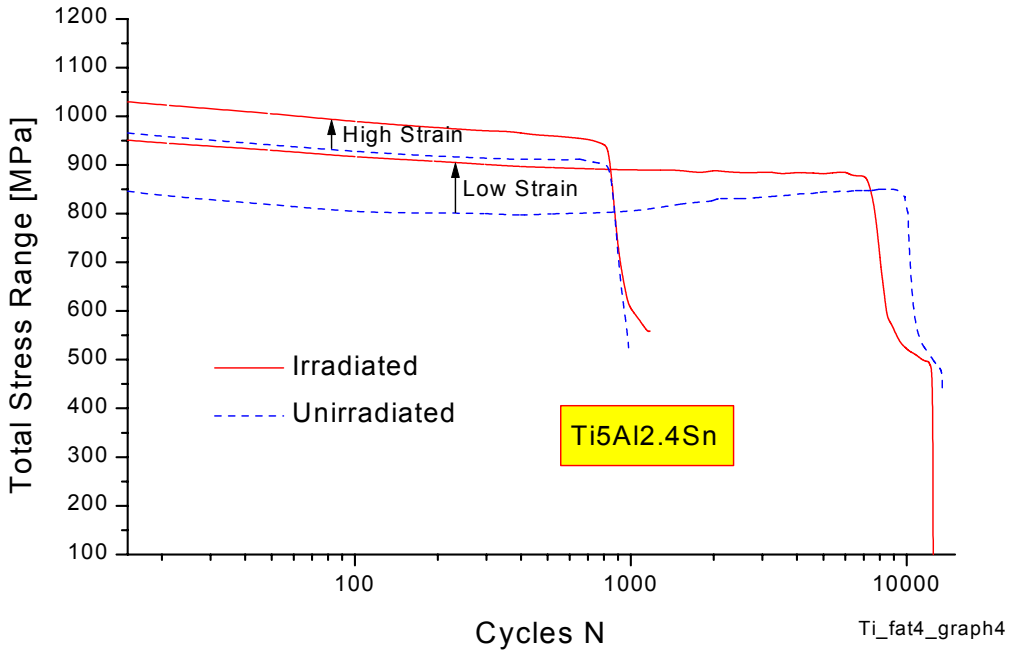

FIGURE 28: The total stress range in unirradiated and irradiated Ti5Al2.5Sn

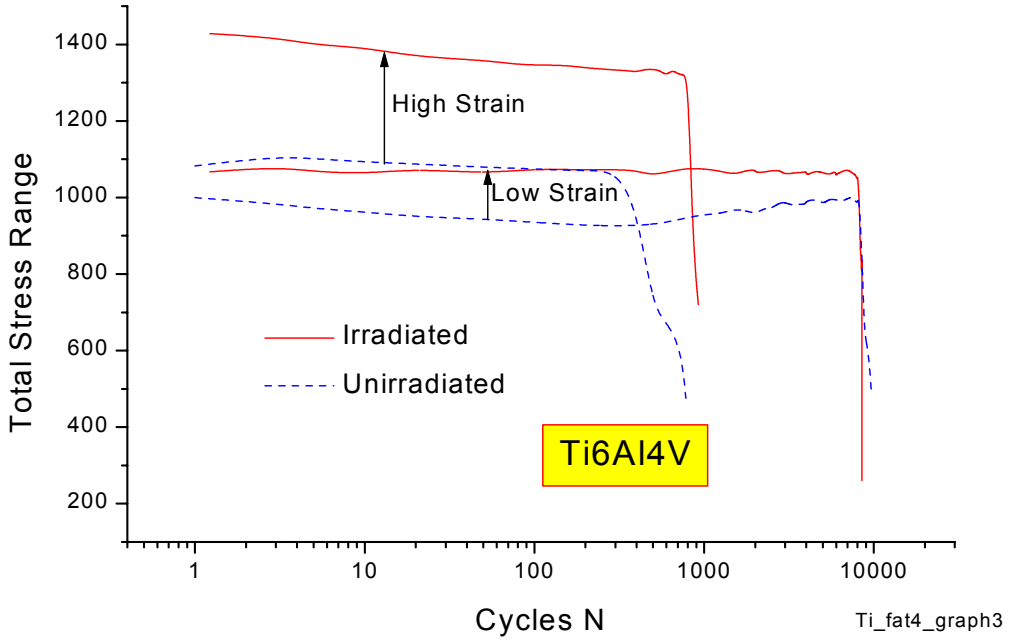

FIGURE 29: The total stress range in unirradiated and irradiated Ti5Al2.5Sn

1.5.3 Cyclic stress asymetry

Another general feature observed in the fatigue testing of both alloys, is the fact that the compressive stress of the hysteresis loop is always higher than the tensile stress. This characteristic seems to be typical for titanium alloys (see also [4]), since it was observed in both alloys and at all the test conditions used in this study, including the irradiated condition. Fig. 30 is a plot of the tensile and compressive stresses observed during the fatigue of the specimen N25F15 (Ti6Al4V, T=350 °C and $\Delta\varepsilon_t$ =1%). The difference of the tensile and compressive stresses is constant during the life.
In order to get a better understanding of this effect, the positive and negative stress amplitudes have been reported for some characteristic conditions in Figs 31 and 32. The largest asymetry observed has a magnitude of 75MPa (Ti6Al4V,1.4%). There seem to be some dependence on the amount of imposed strain and the level of stress. For clarity , the stress asymetry has been plotted as a function of the plastic strain range in Fig. 33, all conditions together. No simple dependence can be found and the figures indicate rather that the asymetry seem to be triggered by the plastic strain. This is in accordance with the absence of asymetry in irradiated Ti6Al4V , cycled at 1% strain , as shown in Fig.31.

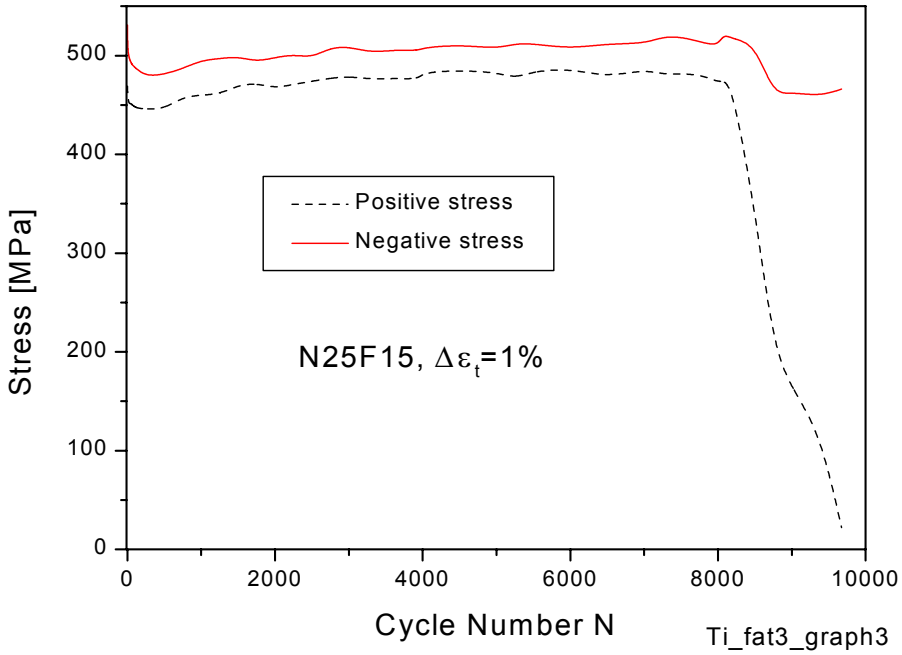

FIGURE 30: The tensile and the compressive stress as a function of the cycle number (T=350 °C and $\Delta\varepsilon_t$ =1%).

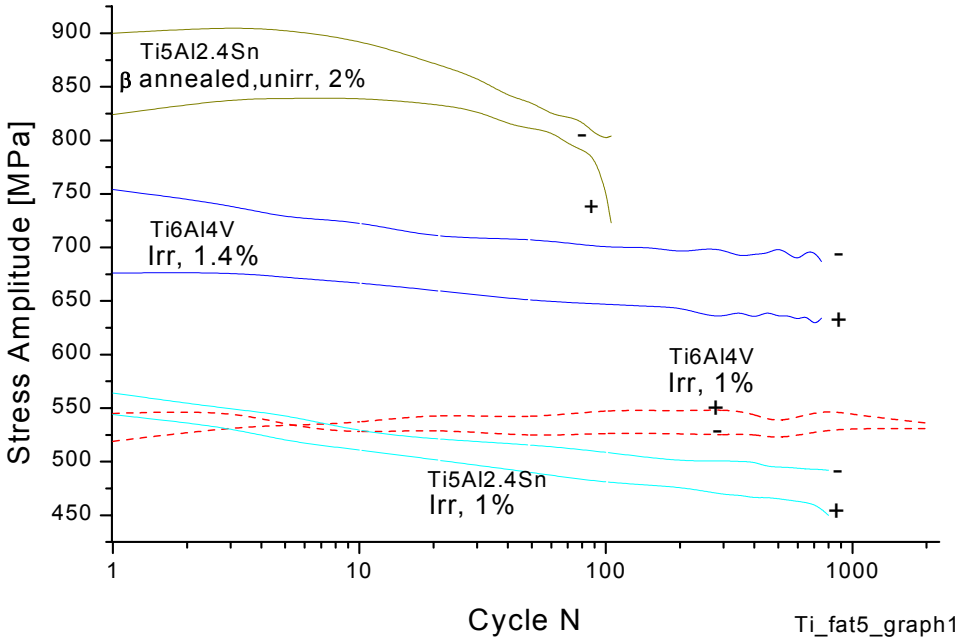

FIGURE 31: Compressive (-) and tensile(+) stress amplitude as a function of cycle number for different conditions.

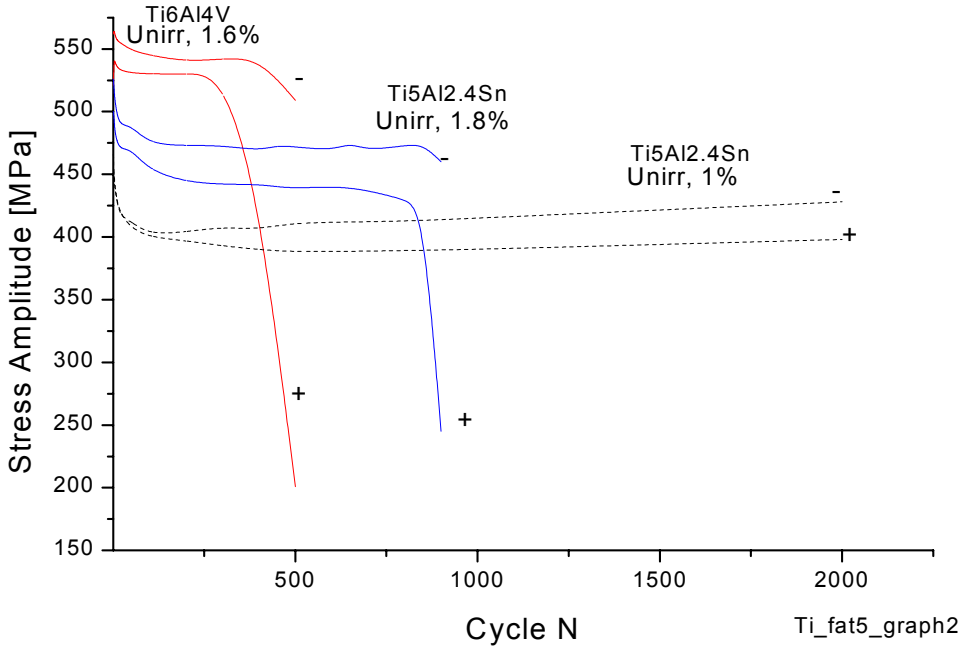

FIGURE 32: Compressive (-) and tensile(+) stress amplitude as a function of cycle number for different conditions.

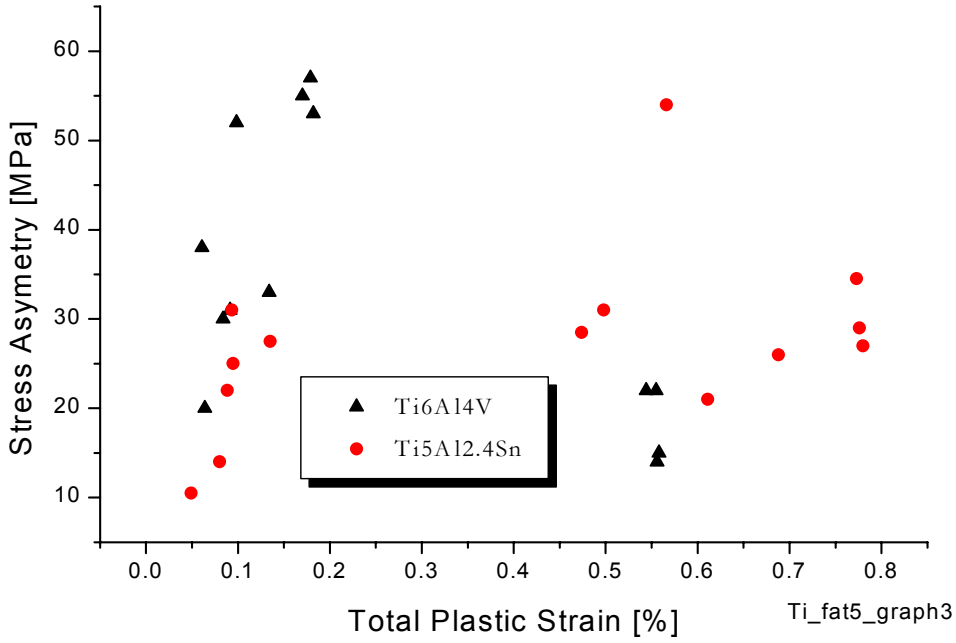

FIGURE 33: Stress asymetry as a function of the plastic strain range

It is difficult to find out what is the reason for this asymetry. Many different mechanisms could be involved like dislocation separation into partials and recombination processes , or different slip systems in tensile and compressive part or even different amount of twinning deformation. A more simple explanation could be that due to the very strong texture of titanium alloys, large quantities of elastic energy is stored into the bulk and released during the tensile cycle. In fact all fatigue specimen were cut along the longitudinal axis of the stock material. Fig.31 shows that the asymetry has survived a beta anneal (1/2h 1055°C,AC,1h,700°C,AC). Since the material was heated above the beta transus, the heat treatment is supposed to have removed at least part of the texture, although it was not measured. More investigations will be necessary to identify the responsible mechanism.

1.5.4 Fatigue endurance

The imposed total strain $\Delta\varepsilon_t$, the total elastic strain $\Delta\varepsilon_e$ and the total plastic strain $\Delta\varepsilon_P$ taken at half life, were plotted as a function of the number of cycles to failure N_f, for both unirradiated materials in Figures 34 and 35.
The strains are taken at half life. The plot enables then the calculation of the coefficients of the fatigue life equation:

$$\Delta\varepsilon_t = \Delta\varepsilon_e + \Delta\varepsilon_p = C_p N_f^{k_p} + C_e N_f^{k_e}$$

The following strain life equations were established:

For Ti 5Al 2.4Sn: $\Delta\varepsilon_t = 260\ N_f^{-0.84} + 1.24\ N_f^{-0.03}$

For Ti 6Al 4V: $\Delta\varepsilon_t = 64\ N_f^{-0.71} + 1.4\ N_f^{-0.04}$

In Fig 36, the strains have been plotted as a function of the number of cycles to crack initiation Na, for the Ti 5Al 2.4Sn. Normally Na is a less dispersed life parameter than Nf and is useful in comparing tests results obtained at the same test conditions.

The endurance of both alloys is compared in Fig.37 where the imposed total strain is represented as a function of Nf. The fatigue resistance appears to be higher in the alpha alloy. This is in accordance with the behavior shown in Fig.25. The higher cyclic stresses in the alpha beta alloy are inducing a higher crack growth rate.

Finally the comparison before and after the irradiation is shown for both alloys in Figs 38 and 39. As shown by the log-log plot, there is no significative degradation of the fatigue of the Ti5Al2.4Sn alloy. In the case of the Ti6Al4V and when the imposed total strain is above 1.2%., the life is clearly reduced by the 0.3dpa/350°C irradiation This reduction is the consequence of the appearance of brittleness as indicated in Table 3.

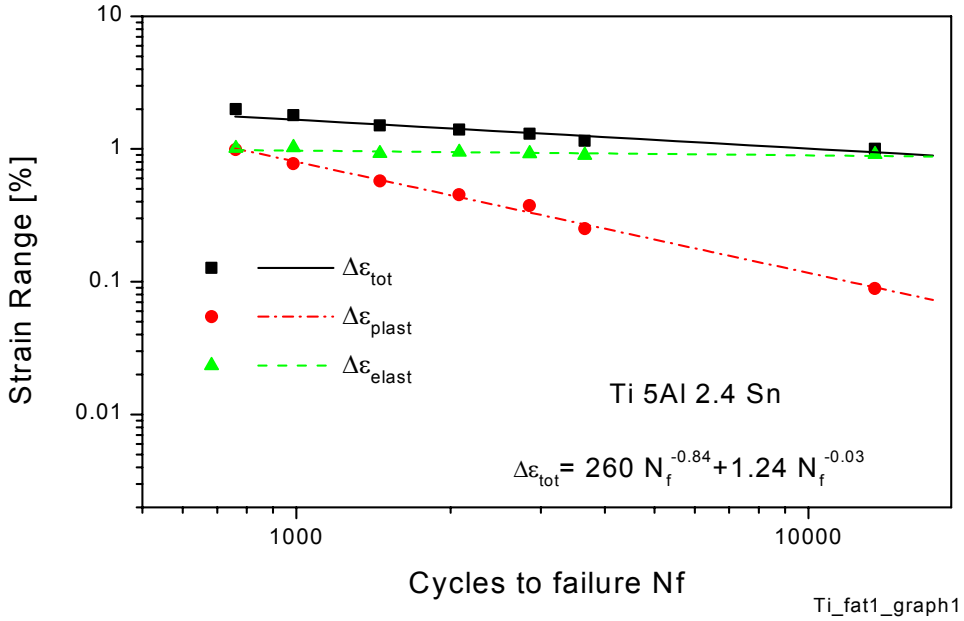

FIGURE 34: The total, elastic and plastic strain ranges as a function of cycles to failure Nf for Ti 5Al 2.4Sn

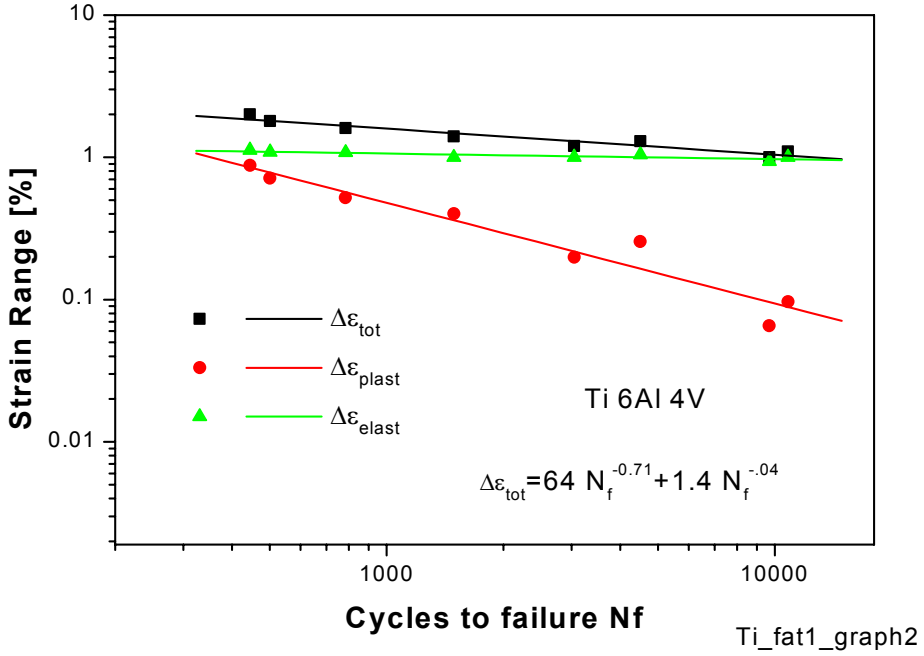

FIGURE 35: The total, elastic and plastic strain ranges as a function of cycles to failure Nf for Ti 6Al 4V

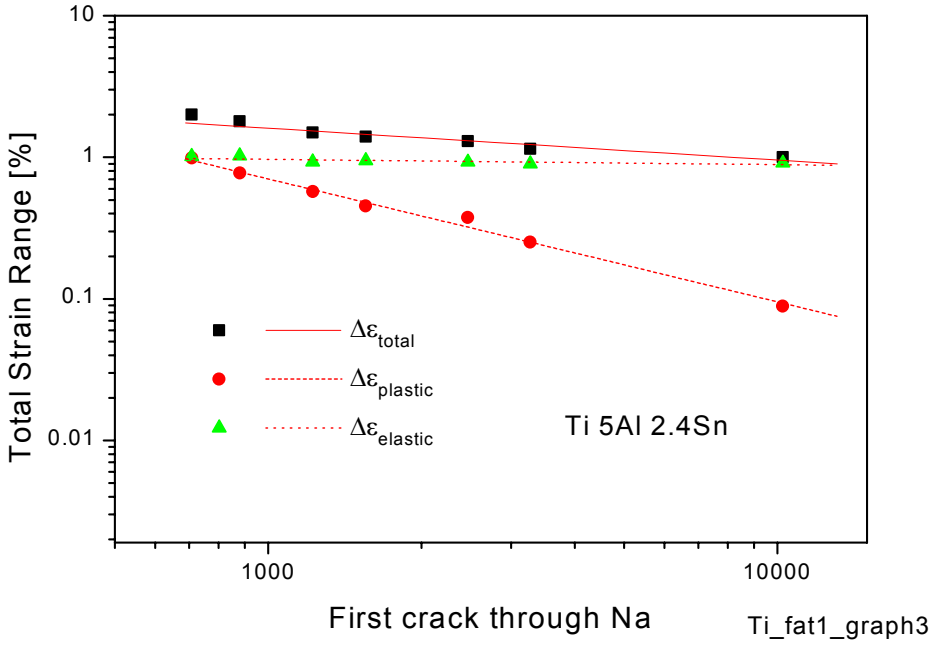

FIGURE 36: The total, elastic and plastic strain ranges as a function of cycles to crack initiation Na for Ti 6Al 4V

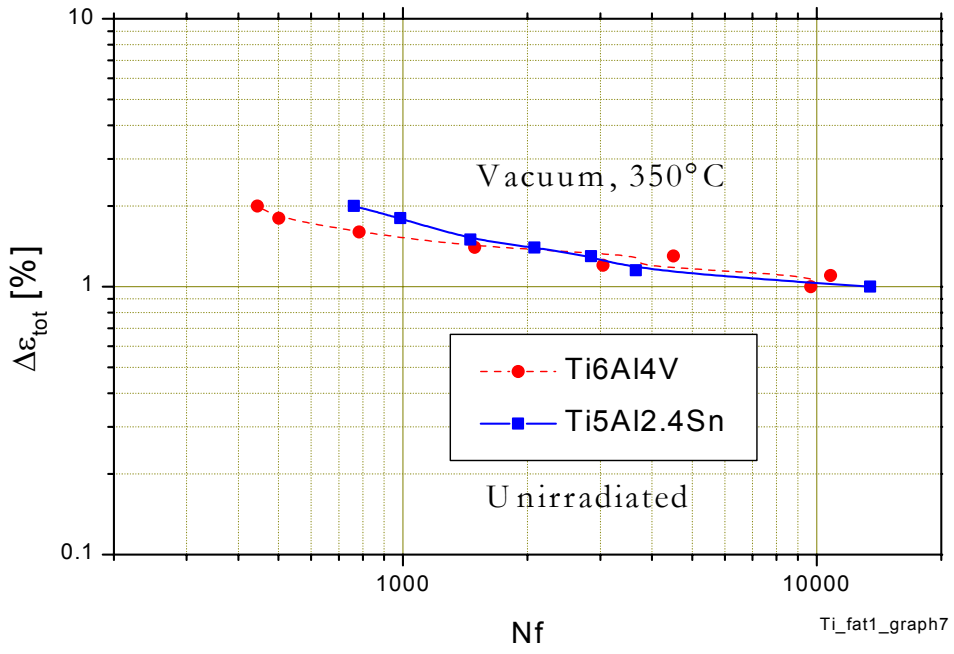

FIGURE 37: Strain life data for Ti 5Al 2.4Sn and Ti 6Al 4V alloys tested at 350°C in vacuum.

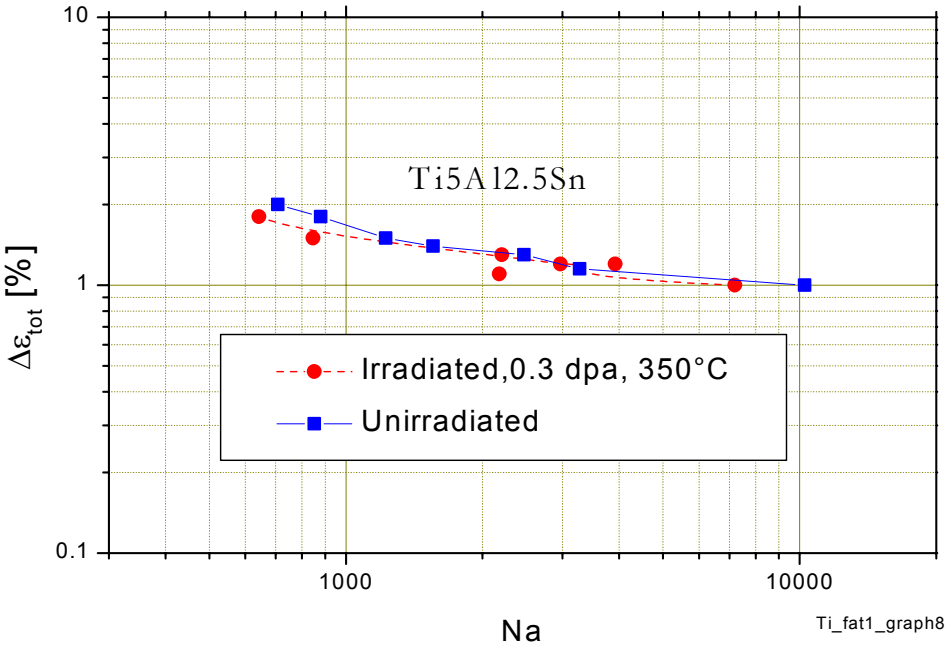

FIGURE 38: Effect of the irradiation on fatigue life of Ti 5Al 2.4Sn alloy tested at 350°C in vacuum.

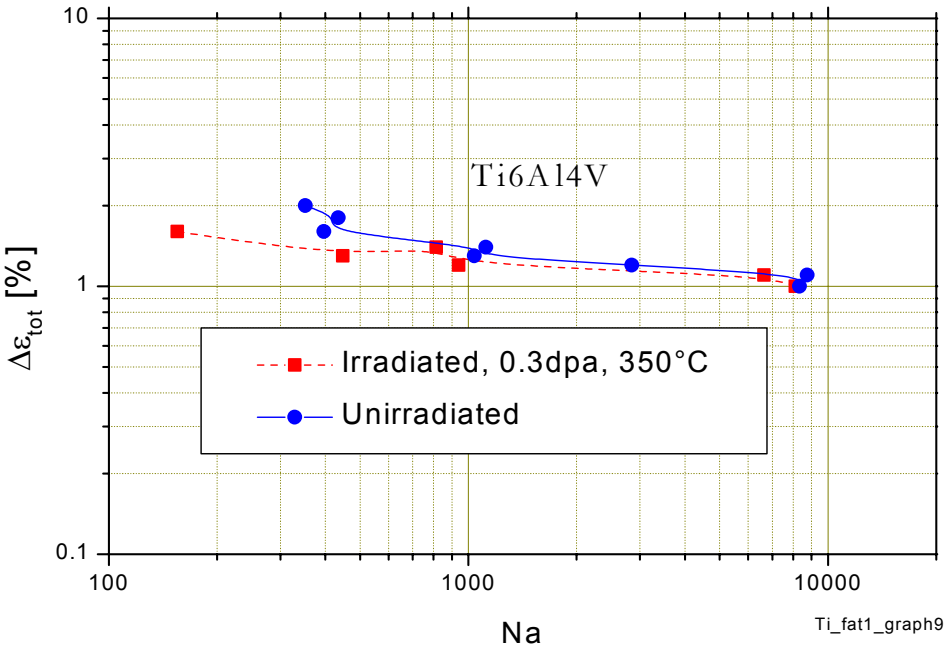

FIGURE 39: Effect of the irradiation on fatigue life of Ti 6Al 4V alloy tested at 350°C in vacuum.

1.5.5 TEM and SEM observations

Figs 40 and 41 show a few TEM micrographs from unirradiated fatigue specimens. Parallel deformation cell walls are formed (Fig 40 left) and deformation induced martensite is generated in the beta grains (Fig. 41 right).

As shown in 1.5.2.1 for low imposed strains, a secondary cyclic hardening is taking place after a classical cyclic softening period (see Fig. 24). This effect may be due to the increasing density of dislocation residues which are produced as a result of the cyclic straining. These debris have been observed in both materials as can be seen in Figs 40 and 41.

In Table 3, the sudden failure of Ti5Al2.5Sn specimen fatigued at RT is reported (N14F20,N14F19,N14F7).To clarify the reasons of this brittleness the fractured surfaces have been looked at in the SEM. It was found that the fracture was transgranular and ductile. No indication of brittleness could be observed. Fig 42 (N14F20) shows a surface that is well plastically deformed and fatigue striations can be found at high magnification at embedded microcracks (Fig. 42 down). Therefore it is believed that the sudden failure of the specimen is due to stress concentration effects in the thin wall specimen (Fig. 6b) and the fact that the stored elastic energy can lead to instabilities (Cyclic stress >1500 MPa).

Two of the irradiated Ti6Al4V specimen also broke in a brittle way. They were tested at 350°C. Again the fracture was transgranular and the fracture surface revealed a ductile behavior (Fig. 43, I25F8). The material is not intrisically brittle but the failure is the result of a local instability.

Brittle features like river patterns or microcracks and small intergranular fractures are observed in both materials in the unirradiated condition (Fig. 44, N14F22, N25F13). The amount of these brittle features increases in the irradiated specimen (Fig. 43, I14F39) which is consistent with the measured reduction of the fatigue life.

1.6 Conclusions

Tensile tests:

The testing of the irradiated materials being done with subsize specimen, two series of tests were conducted on DIN normed specimen. The results show that the measured stresses in the subsize specimen are smaller by less than 11% and that the differences observed are temperature dependent.
The ductilities observed in the DIN specimen are higher, specially at room temperature.
The tensile resistance of both studied alloys is very similar. The $\sigma_{0.2}$ stress has a value around 800 MPa at RT and 450MPa at 350°C. At temperatures up to 150°C, the alpha alloy Ti5Al2.4Sn is slightly superior to the alpha+beta alloy. The reverse takes place at higher temperatures. The total elongation is slightly higher in the alpha+beta alloy as compared to the alpha alloy.
The alpha+beta structure is more stable and resist better to an heat treatment of 5hrs/750°C.

Effects of irradiation:

The irradiation hardening is much stronger in the alpha+beta alloy as compared to the alpha alloy (250MPa-50MPa at RT). Accordingly the loss of ductility is more pronounced in the alpha+beta alloy. The irradiation hardening is athermal and long range in nature.
In the alpha alloy, the low temperature irradiation reduced the strain hardening capability. The yield point has been eliminated and DSA has been slightly enhanced by the irradiation.
The different amount of irradiation hardening observed in the two alloy systems may be connected to differences in the incubation kinetics of the point defects.
The dose of 0.3 dpa has already produced drastic effects , specially for the case of the alpha +beta alloy . Despite the fact that all fractures were ductile at the strain rate range studied, irradiation embrittlement at a higher strain rate could be a concern.

Fatigue tests at 350°C:

Two different regimes have been observed in the behavior of the cyclic stresses. At a high imposed strain, the softening is almost absent in the Ti 6Al 4V and small in the Ti5Al2.4 Sn. At a low imposed strain and for both alloys, during the first period of life, cyclic softening is taking place (up to about 800 cycles). But then a transition occurs after which a regime of cyclic hardening appears. The TEM observations have shown that the secondary hardening may be due to dislocation interactions with dislocation debris.
In both materials and for all test conditions, the compressive stress of the hysteresis loop was found to be larger than the tensile stress. This characteristic has been observed for all tested conditions, in both alloys. A beta anneal did not suppress it. The stress asymetry seems to be triggered by the plastic deformation.

The fatigue resistance of the Ti 5Al 2.4Sn alloy is slightly better than that of the Ti 6Al 4V alloy.

Effects of irradiation:

The behavior of the cyclic stresses has been changed by the irradiation. The hardening regime was absent in the irradiated specimen. The cyclic stresses were generally higher in the system alpha+beta.
The fatigue endurance performance is superior in the Ti5Al2.5Sn as compared to the Ti6Al4V alloy.
The SEM micrographs have shown that all fractures were transgranular and ductile.

Acknowledgements:

The Paul Scherrer Institute at Villigen, PSI and many of its collaborators are sincerely thanked for their logistical and technical support and scientific collaboration throughout this project.

REFERENCES:

[1] P.Marmy et al., PIREX II - A New Irradiation Facility for Testing Fusion First Wall Materials, Nuclear Instruments and Methods in Physics Research B47 (1990)37-47.
[2] Sherron L. Green, Calculated Radiation Damage Effects of High Energy Proton Beams, J. of Nucl. Materials 126 (1984)30-37.
[3] A.A.F. Tavassoli, J. of Nucl. Mater. 258-263(1998)85-96
[4] A.S. Beranger, X. Feaugas and M. Clavel, Mater. Science and Eng., A172(1993)31-41